The contribution of the magnetic quadrupole to the angular distribution and polarization of electron-impact excitation and dielectronic recombination in highly charged ions



2015 J. Phys. B: At. Mol. Opt. Phys. 48 144005

(http://iopscience.iop.org/0953-4075/48/14/144005)

IOP Publishing Journal of Physics B: Atomic, Molecular and Optical Physics
J. Phys. B: At. Mol. Opt. Phys. **48** (2015) 144005 (9pp) doi:10.1088/0953-4075/48/14/144005

# The contribution of the magnetic quadrupole to the angular distribution and polarization of electron-impact excitation and dielectronic recombination in highly charged ions

**Z B Chen[1], J L Zeng[1], H W Hu[2] and C Z Dong[3]**

[1] College of Science, National University of Defense Technology, Changsha, Hunan 410073, People's Republic of China
[2] Department of Physics, Shangqiu Normal University, Shangqiu, 476000, People's Republic of China
[3] Key Laboratory of Atomic and Molecular Physics & Functional Materials of Gansu Province and Northwest Normal University, Lanzhou, 730070, People's Republic of China

E-mail: chenzb008@qq.com and jlzeng@nudt.edu.cn

Received 30 October 2014, revised 30 December 2014
Accepted for publication 5 January 2015
Published 28 May 2015

**Abstract**

The degree of linear polarization and angular distribution of the x-ray photoemission of highly charged He-like and Li-like uranium ions following electron-impact excitation and dielectronic recombination processes are calculated using a fully relativistic distorted-wave method. A detailed investigation is carried out regarding the contribution of the magnetic quadropole ($M2$) term to the subsequent characteristic x-ray emission from the above two different processes. It is found that while the $M2$ term has a slight effect on the angular distribution and linear polarization of electron-impact excitation, it has a substantial effect on the same properties of dielectronic recombination.

Keywords: linear polarization, electron-impact excitation, dielectronic recombination

## 1. Introduction

The polarization of x-ray line emission from highly charged ions undergoing collisions with an electron beam has been a topic of continuous fundamental interest for decades [1–8]. From the polarization and angular distribution of decay products following the collision process, valuable information can be obtained regarding both the collision dynamics and the magnetic sublevel population of the impact-excited states, which becomes indispensable for the detailed diagnosis of the plasma state and the analysis of the complex spectra formation mechanism [8]. In recent years, some important diagnostic tools have been successfully developed and applied to describe both the angular distribution and the polarization properties of x-ray emission existing in astrophysical and laboratory plasmas, particularly in solar corona plasmas [1, 2], tokamak plasmas [3] and laser-produced plasmas [4–6].

Several studies have been carried out in the past to better understand the role of angular and polarization properties associated to different processes. With respect to electron-impact excitation (EIE) processes, Reed *et al* [9] investigated the relativistic effects on the linear polarization of radiation emitted following EIE of highly charged H-like and He-like ions. They found that relativistic effects considerably alter the linear polarization, and that the changes resulting from relativistic effects become progressively more significant as the incident-electron energy and/or the atomic number increases. Hakel *et al* [10] calculated x-ray line polarization degrees for cases with axial symmetry using a collisional-radiative magnetic-sublevel atomic kinetics model. They also studied the cascade effects on the linear polarization of He-like $Fe^{24+}$

 

ions. Sharma *et al* [11] investigated the degree of linear polarization of the $ns_{1/2}$-$np_{1/2}$ and $ns_{1/2}$-$np_{3/2}$ resonance transitions after EIE for several single charged ions. Inal *et al* [12] have studied the hyperfine interaction effects on the polarization of He-like $Sc^{19+}$ ions. With respect to dielectronic recombination (DR) processes, Fritzsche *et al* [13] calculated the linear polarization of Be-like ions. They found that the Breit interaction, as the dominant correction to the Coulomb repulsion, may lead to a qualitative change in linear polarization. This predicted phenomenon has recently been observed and confirmed experimentally [14]. Matula *et al* [15] investigated the angular correlations between the photons emitted in the DR of H-like $U^{91+}$ ions. They found that the higher multipole components can notably modify the angular properties of the radiative cascades between the fine-structure levels by up to 35%. Wu *et al* [16] calculated the linear polarization of the two strongest $5f \rightarrow 3d$ lines of Cu-like to Se-like gold ions, and they found that the polarizations following the EIE and DR processes are totally different. There have also been many studies on the linear polarization from other dynamical processes [17–30].

Until now, however, almost all theoretical studies of linear polarization have dealt with a single multipole term only, either purely electric or purely magnetic. Little attention has been paid so far to the contributions of the multipole decay to the polarization properties. As pointed out in [31], even if one of the multipoles contributes about 1% to the total transition probability, the angular distribution of radiation can be significantly affected by the interference between multipoles. Early work on the non-electric dipole ($E1$) effects on the characteristic x-ray emission was performed by Fritzsche and co-workers [15, 32–34]. In these investigations, the multipole-mixing effects and the interference effects were studied following the DR process. The results showed that the interference between the leading $E1$ and other electric and magnetic multipoles may significantly alter the angular distribution and linear polarization of the emitted x-rays [33]. Such strong interference effects between the $E1$ and $M2$ transitions have been also found for Lyman-$\alpha_1$ decay of H-like $U^{91+}$ ions [35] following radiative electron capture (REC). And these effects, especially the $M2$ contributions, can reduce the angular distribution of linear polarization by about 16% when compared with the pure $E1$ decay approximation. This was confirmed experimentally with the heavy-ion storage ring facility at GSI-Darmstadt [35]. Therefore, similar effects should also be expected for x-ray emissions from other dynamical processes. On the other hand, with the recent advancements in the design of position-sensitive solid state detectors [35], these studies have become feasible. Detailed theoretical predictions are thus required in order to select candidate systems and to interpret their outcome [8].

In this contribution we apply the multi-configuration Dirac–Fock (MCDF) method and fully relativistic distorted-wave (RDW) method to explore an interference between the $E1$ and the $M2$ transition for the $2s_{1/2}\ 3p_{3/2}(J = 1) \rightarrow 1s_{1/2}2s_{1/2}(J = 1)$ line of He-like $U^{90+}$ ions and the $1s_{1/2}2s_{1/2}2p_{3/2}(J = 3/2) \rightarrow 1s^2 2s_{1/2}(J = 1/2)$ line of Li-like $U^{89+}$ ions formed by EIE and DR processes, respectively. Special attention is paid to the contributions of $M2$ decay to the polarization properties and angular distribution of radiation for subsequent x-ray emission from these two different processes. To perform such an analysis, in section 2, we provide a detailed description of the theoretical method and computational procedure. In section 3 we then present our results for the effects of $E1$-$M2$ interference on the polarization and angular distribution of x-ray radiation. Differences between the interference effects on the EIE and DR processes are analyzed in terms of the atomic number and the incident energy. Finally, some brief conclusions are given in section 4.

## 2. Theoretical method

In this study, the atomic structure data used in calculating cross sections are generated using the MCDF method and the corresponding computational packages GRASP92 [36]. The continuum electron wave functions are produced by the component COWF of the RATIP package [37]. The cross sections for EIE and DR of individual magnetic sublevels of He-like and Li-like ions are calculated using a fully RDW program [20, 38, 39].

### 2.1. Calculations of EIE processes

In the RDW method, the $z$ axis is taken along the incident electron beam, so the $z$ component of the incident electron orbital angular momentum $m_{l_i} = 0$. Then, the direct EIE cross sections of the target ion from $\beta_i J_i M_i$ to $\beta_f J_f M_f$ can be written as [16, 20, 40]

$$\begin{aligned}
&\sigma_{\varepsilon_i}\left(\beta_i J_i M_i - \beta_f J_f M_f\right) \\
&= \frac{2\pi a_0^2}{k_{i^2}} \cdot \sum_{l_i, l_i', j_i, j_i', m_{s_i}, l_f, j_f, m_f} \\
&\times \sum_{J, J', M} (i)^{l_i - l_i'} \left[\left(2l_i + 1\right)\left(2l_i' + 1\right)\right]^{1/2} \\
&\times \exp\left[i\left(\delta_{\kappa_i} - \delta_{\kappa_i'}\right)\right] C\left(l_i \frac{1}{2} m_{l_i} m_{s_i}; j_i m_i\right) \\
&\times C\left(l_i' \frac{1}{2} m_{l_i'} m_{s_i}; j_i' m_i\right) C\left(J_i j_i M_i m_i; JM\right) \\
&\times C\left(J_i j_i' M_i m_i; J'M\right) C\left(J_f j_f M_f m_f; JM\right) \\
&\times C\left(J_f j_f M_f m_f; J'M\right) R(\gamma_i, \gamma_f) R\left(\gamma_i', \gamma_f'\right), \qquad (1)
\end{aligned}$$

Here, the subscripts i and f denote the initial and final states, $\varepsilon_i$ is the incident electron energy in Rydbergs and $a_0$ is the first Bohr radius. The $C$'s are Clebsch–Gordan coefficients.

$$\gamma_i = \varepsilon_i l_i j_i \beta_i J_i JM; \ \ \gamma_f = \varepsilon_f l_f j_f \beta_f J_f JM \qquad (2)$$

in which $\beta_i(\beta_f)$ represents other quantum numbers which are required to specify the initial (final) states of the target ion in addition to the total angular momentum $J_i(J_f)$ and its $z$ component $M_i(M_f)$, respectively. $J$ and $M$ are the quantum numbers corresponding to the total (target ion plus free electron) angular momentum of the complete system, and its $z$

component, respectively; $m_{s_i}$ and $m_{l_i}$ are the spin and the orbital angular momentum of the incident electron, respectively. $j_i$ and $m_i$ are the total angular momentum and its $z$ component of the incident electron, respectively. $\kappa$ is the relativistic quantum number. $\delta_{\kappa_i}$ is the phase shift for the continuum electron. $k_i$ is the relativistic wave number of the incident electron, and is given by [16]

$$k_i^2 = \varepsilon_i\left(1 + \frac{\alpha^2\varepsilon_i}{4}\right), \tag{3}$$

in which $\alpha$ is the fine-structure constant. The collision matrix element $R(\gamma_i, \gamma_f)$ can be written as

$$R(\gamma_i, \gamma_f) = \left\langle \Psi_{\gamma_f}\middle| \sum_{p,q,p<q}^{N+1} \left(V_{\rm Coul} + V_{\rm Breit}\right)\middle|\Psi_{\gamma_i}\right\rangle, \tag{4}$$

where $V_{\rm Coul}$ ($V_{\rm Breit}$) is the Coulomb (Breit) interaction operator [36]. $\Psi_{\gamma_i}$ and $\Psi_{\gamma_f}$ are the initial and final states wavefunctions of the impact systems, respectively. In the calculations, one can average over $M_i$ of the target ion and obtain the cross section for excitation to a specific final magnetic sublevel $M_f$.

### 2.2. Calculations of DR processes

In the DR process, the quantization axis is defined as in section 2.1, and the capture cross section from $i$ (initial state) to the magnetic sublevels of $f$ (final state, doubly excited state) can be written as [16]

$$\begin{aligned}&\sigma_{\varepsilon_i}^{cap}\left(\beta_i J_i M_i - \beta_f J_f M_f\right)\\ &= S^{\rm cap}\left(\beta_i J_i M_i - \beta_f J_f M_f\right)\delta(\varepsilon_i - \varepsilon_{if}),\end{aligned} \tag{5}$$

where

$$\begin{aligned}&S^{\rm cap}\left(\beta_i J_i M_i - \beta_f J_f M_f\right)\\ &= \frac{2\pi a_0^2}{k_i{}^2}\cdot \sum_{l_i,l_i',j_i,j_i',m_{s_i}} (\mathrm{i})^{l_i-l_i'}\left[\left(2l_i+1\right)\left(2l_i'+1\right)\right]^{1/2}\\ &\times \exp\left[\mathrm{i}\left(\delta_{\kappa_i} - \delta_{\kappa_i'}\right)\right] C\left(l_i\,\frac{1}{2}\,0m_{s_i};\, j_i m_i\right)\\ &\times C\left(l_i'\,\frac{1}{2}\,0m_{s_i};\, j_i' m_i\right) C\left(J_i j_i M_i m_i;\, J_f M_f\right)\\ &\times C\left(J_i j_i' M_i m_i;\, J_f M_f\right) R(\gamma_f, \gamma_i) R\left(\gamma_f', \gamma_i'\right).\end{aligned} \tag{6}$$

### 2.3. Calculations of E1-M2 interference effects

For radiation from the $J = 3/2$ level to the $J = 1/2$ level and from the $J = 1$ level to the $J = 1$ level, the linear polarization at the observation angle can be written as [41]

$$\eta(\theta) = \frac{P\sin^2\theta}{1 - g(E1, M2)P\cos^2\theta}. \tag{7}$$

Here, $P$ is the degree of linear polarization at the observation angle of 90° in the ion-rest frame,

$$P = \frac{A}{B + C}. \tag{8}$$

For radiation from the $J = 3/2$ level to the $J = 1/2$ level,

$$A = (\sigma_{1/2} - \sigma_{3/2})\left(3A_{E1} - 3A_{M2} + 2\sqrt{3A_{E1}A_{M2}}\right), \tag{9}$$

$$B = \left(5\sigma_{1/2} + 3\sigma_{3/2}\right)A_{E1} + \left(3\sigma_{1/2} + 5\sigma_{3/2}\right)A_{M2}, \tag{10}$$

$$C = 2(\sigma_{1/2} - \sigma_{3/2})\sqrt{3A_{E1}A_{M2}}, \tag{11}$$

and

$$g(E1, M2) = \frac{A_{E1} - A_{M2} + 2\sqrt{3}\sqrt{A_{E1}A_{M2}}}{A_{E1} - A_{M2} - 2\frac{\sqrt{3}}{3}\sqrt{A_{E1}A_{M2}}}. \tag{12}$$

The angular distribution of x-ray radiation is given by

$$\begin{aligned}W(\theta) = \langle W\rangle\Bigg\{1 + \Bigg[&\frac{A_{E1} - A_{M2} + 2\sqrt{3}\sqrt{A_{E1}A_{M2}}}{A_{E1} + A_{M2}}\\ &\times \frac{1}{2}\frac{\sigma_{3/2} - \sigma_{1/2}}{\sigma_{3/2} + \sigma_{1/2}} P_2\left(\cos\theta\right)\Bigg]\Bigg\},\end{aligned} \tag{13}$$

where $A_{E1}$ ($A_{M2}$) is the pure $E1$ ($M2$) transition probability. $\langle W\rangle$ and $P_2(\cos\theta)$ are the mean intensity [41] and the second-order Legendre polynomial, respectively. $\sigma_{1/2}$ and $\sigma_{3/2}$ are the EIE or DR cross sections from the initial state to the final magnetic sublevels $M_f = 1/2$ and 3/2, respectively.

For the $J = 1$ to $J = 1$ lines,

$$A = (\sigma_1 - \sigma_0)\left(A_{E1} + A_{M2} + 2\sqrt{A_{E1}A_{M2}}\right), \tag{14}$$

$$B = \left(\sigma_0 + 3\sigma_1\right)\left(A_{E1} + A_{M2}\right), \tag{15}$$

$$C = 2(\sigma_0 - \sigma_1)\sqrt{A_{E1}A_{M2}}, \tag{16}$$

and

$$g(E1, M2) = \frac{A_{E1} + A_{M2} - 6\sqrt{A_{E1}A_{M2}}}{A_{E1} + A_{M2} + 2\sqrt{A_{E1}A_{M2}}}. \tag{17}$$

The angular distribution of x-ray radiation is given by

$$\begin{aligned}W(\theta) = \langle W\rangle\Bigg\{1 + \Bigg[&\frac{A_{E1} + A_{M2} - 6\sqrt{A_{E1}A_{M2}}}{A_{E1} + A_{M2}}\\ &\times \frac{1}{2}\frac{\sigma_0 - \sigma_1}{\sigma_0 + 2\sigma_1} P_2\left(\cos\theta\right)\Bigg]\Bigg\},\end{aligned} \tag{18}$$

where $\sigma_0$ and $\sigma_1$ are the EIE or DR cross sections from the initial state to magnetic sublevels $M_f = 0$ and 1 of the final state, respectively.

### 2.4. Details of the calculation

In this study, for the $1\,s_{1/2}2s_{1/2}2p_{3/2}(J = 3/2) \rightarrow 1s^2 2s_{1/2}$ ($J = 1/2$) transition line of Li-like ions, the DR process can be

**Table 1.** Comparison of the transition probabilities ($s^{-1}$) of the $2s_{1/2}3p_{3/2}(J=1) \rightarrow 1s_{1/2}2s_{1/2}(J=1)$ line of He-like $U^{90+}$ ions and the $1\,s_{1/2}2s_{1/2}2p_{3/2}(J=3/2) \rightarrow 1s^2 2s_{1/2}(J=1/2)$ line of Li-like $U^{89+}$ ions between the present calculated results and the existing theoretical results. Superscript B: Babushkin gauge; superscript C: Coulomb gauge. $R$[n] means $R \times 10^n$.

| Ions | Type | Present | Others |
|---|---|---|---|
| | | He-like | |
| $Ho^{65+}$ | $E1$ | 1.03[15]$^{C}$, 1.05[15]$^{B}$ | |
| | $M2$ | 7.33[12] | |
| $U^{90+}$ | $E1$ | 3.12[15]$^{C}$, 3.37[15]$^{B}$ | 3.94[15]$^{a}$ |
| | $M2$ | 9.94[13] | |
| | | Li-like | |
| $Fe^{23+}$ | $E1$ | 3.92[12]$^{B}$, 4.22[12]$^{B}$ | 4.40[12]$^{b}$, 4.43[12]$^{c}$ |
| | $M2$ | 5.52[8] | |
| $U^{89+}$ | $E1$ | 1.05[16]$^{C}$, 1.14[16]$^{B}$ | 1.06[16]$^{a}$ |
| | $M2$ | 1.41[14] | |

[a] [42]
[b] [44]
[c] [45]

described schematically by

$$\varepsilon e + 1s^2 \rightarrow 1s_{1/2}2s_{1/2}2p_{3/2}(J=3/2) \rightarrow 1s^2 2s_{1/2}(J=1/2) + h\nu. \quad (19)$$

The same transition line of Li-like ions can also be formed by the inner-shell EIE process

$$\varepsilon e + 1s^2 2s_{1/2}(J=1/2) \rightarrow 1s_{1/2}2s_{1/2}2p_{3/2}(J=3/2) + \varepsilon' e \rightarrow 1s^2 2s_{1/2}(J=1/2) + h\nu. \quad (20)$$

Similarly, for the $2s_{1/2}3p_{3/2}(J=1) \rightarrow 1s_{1/2}2s_{1/2}(J=1)$ transition line of He-like ions, the DR process can be described schematically by

$$\varepsilon e + 1s_{1/2} \rightarrow 2s_{1/2}3p_{3/2}(J=1) \rightarrow 1s_{1/2}2s_{1/2}(J=1) + h\nu. \quad (21)$$

For the same transition line, the EIE process can be described by

$$\varepsilon e + 1s_{1/2}2s_{1/2}(J=1) \rightarrow 2s_{1/2}3p_{3/2}(J=1) + \varepsilon' e \rightarrow 1s_{1/2}2s_{1/2}(J=1) + h\nu. \quad (22)$$

## 3. Results and discussions

### 3.1. Transition probabilities and cross sections

To obtain accurate energy levels and wave functions of the initial and final states, the contributions of the Breit interaction and quantum electrodynamics (QED) corrections (self-energy and vacuum polarization) are taken into account [16]. Furthermore, in the calculations of the EIE and DR cross sections, the maximal partial-wave $\kappa = 90$ is included in order to ensure convergence. In table 1, the calculated transition probabilities for the $2s_{1/2}3p_{3/2}(J=1) \rightarrow 1s_{1/2}2s_{1/2}(J=1)$ transition line of He-like ions and the $1s_{1/2}2s_{1/2}2p_{3/2}(J=3/2) \rightarrow 1s^2 2s_{1/2}(J=1/2)$ transition line of Li-like ions are listed along with the existing theoretical values. It can be seen that the agreement with the different calculations is good in general. The present $E1$ transition probabilities $3.12 \times 10^{15}$ and $1.05 \times 10^{16}$ $s^{-1}$, are in good agreement with the $E1$ results $3.94 \times 10^{15}$ and $1.06 \times 10^{16}$ $s^{-1}$ listed in the NORAD Atomic Data [42] (calculations of Nahar *et al* [43] for He-like $U^{90+}$ and Li-like $U^{89+}$ ions, respectively). In addition, the present transition probabilities in different gauges (Babushkin and Coulomb) are also reasonably consistent with each other.

EIE and capture cross sections for He-like and Li-like uranium ions are presented in table 2. As for the $1s_{1/2}2s_{1/2}(J=1) \rightarrow 2s_{1/2}3p_{3/2}(J=1)$ excitation, both total and magnetic cross sections decrease as impact energy increases; they decrease rapidly near the threshold energy but slowly within a higher energy region. The magnetic sublevel $M_f = 0$ is preferentially populated in this excitation process. This character is similar to the case of the $1s^2 2s_{1/2}(J=1/2) \rightarrow 1s_{1/2}2s_{1/2}2p_{3/2}(J=3/2)$ and other excitations [9, 26], where the magnetic sublevels with the smaller magnetic quantum number are preferentially populated. It is worth mentioning that for the EIE of Be-like ions [39], the sublevel $M_f = 0$ is preferable for lower impact energies but for higher energies the sublevel $M_f = 1$ is preferable. For the DR process, the capture cross sections are significantly larger than those EIE

**Table 2.** Total and magnetic sublevel cross sections ($cm^2$) of He-like and Li-like uranium ions for EIE and DR processes. $X$ is the incident electron energy in threshold units; for He-like $U^{90+}$ ions, $X = 118537$ eV; for Li-like $U^{89+}$ ions, $X = 100848$ eV. $R$[n] means $R \times 10^n$.

| | | He-like $U^{90+}$ ions | | | Li-like $U^{89+}$ ions | | |
|---|---|---|---|---|---|---|---|
| Process | Energy(X) | $\sigma_0$ | $\sigma_1$ | Total | $\sigma_{1/2}$ | $\sigma_{3/2}$ | Total |
| EIE | 1.2 | 2.17[−26] | 1.94[−26] | 6.05[−26] | 1.25[−25] | 6.54[−26] | 3.81[−25] |
| | 1.5 | 1.31[−26] | 1.64[−26] | 4.59[−26] | 1.03[−25] | 6.06[−26] | 3.27[−25] |
| | 2 | 7.70[−27] | 1.43[−26] | 3.62[−26] | 8.43[−26] | 5.94[−26] | 2.87[−25] |
| | 2.5 | 5.96[−27] | 1.28[−26] | 3.15[−26] | 7.14[−26] | 6.05[−26] | 2.64[−25] |
| | 3 | 5.43[−27] | 1.20[−26] | 2.95[−26] | 6.58[−26] | 6.29[−26] | 2.57[−25] |
| DR | | 3.28[−21] | 1.04[−21] | 4.32[−21] | 3.00[−20] | 0 | 6.00[−20] |

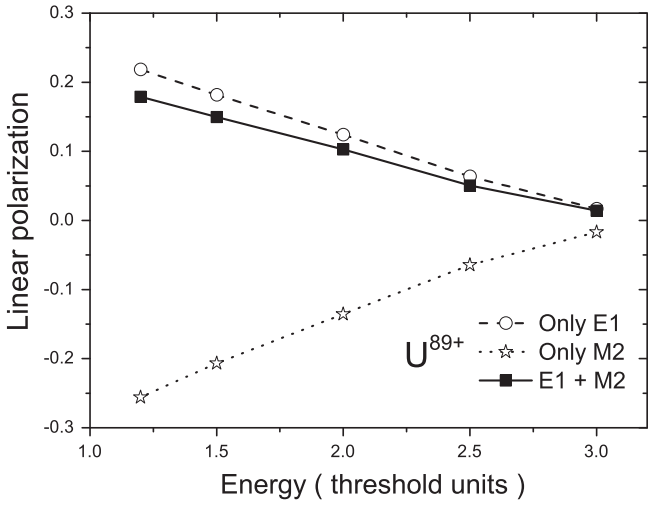


**Figure 1.** The linear polarization at the observation angle of 90° for the transition line $1s_{1/2}2s_{1/2}\,2p_{3/2}\,(J = 3/2) \rightarrow 1s^2 2s_{1/2}(J = 1/2)$ of Li-like $U^{89+}$ ions following the EIE process as functions of the incident electron energy in threshold units. E1 represents inclusion of only the electric-dipole approximation, M2 represents inclusion of only the magnetic-quadrupole approximation, and E1+M2 represents values with inclusion of *E*1-*M*2 interference.

cross sections at all given incident electron energies besides the $\sigma_{3/2}$ magnetic cross sections, which are equal to constant 0. The reason is that the total angular momentum of the incident electron is $\pm 1/2$ in the present method, and the total angular momentum of the capture final state will only change by $\pm 1/2$ when compared with the total angular momentum of the capture initial state.

### *3.2. The contributions of the magnetic quadrupole to Li-like $U^{89+}$ ions*

Using the atomic data displayed in tables 1 and 2, we calculated the degree of linear polarization for the $1s_{1/2}2s_{1/2}2p_{3/2}$ $(J = 3/2) \rightarrow 1s^2 2s_{1/2}(J = 1/2)$ transition line of Li-like $U^{89+}$ ions and each of its components using equations (7)–(12). Figure 1 shows the influence of *E*1-*M*2 interference on the linear polarization as functions of incident electron energy following the EIE process. For comparison, we also show in this figure the results only with purely electric and purely magnetic transitions. As shown in figure 1, the polarization of the *E*1 component decreases while the *M*2 component increases as the incident electron energy increases. The *E*1-*M*2 interference has a larger effect and decreases the linear polarization for the *E*1 component. This effect becomes less important as the incident electron energy increases. The contributions of *E*1-*M*2 interference effects on the linear polarization of the *E*1 component for Li-like $U^{89+}$ ions are about 14% at 1.2 times the threshold energy.

DR of He-like $U^{90+}$ ions can also form the same excited states formed in EIE of $U^{89+}$ ions. In figure 2, the polarizations for the $1s_{1/2}\ 2s_{1/2}\ 2p_{3/2}(J = 3/2) \rightarrow\ 1s^2 2s_{1/2}(J = 1/2)$ transition line of Li-like ions at 1.2 times the threshold energy formed by EIE and DR processes are displayed versus the atomic number, respectively. For the EIE process, as shown in figure 2(a), the linear polarization of the *E*1 component decreases while the *M*2 component increases as the atomic number increases. The *E*1-*M*2 contribution causes the *E*1 contribution to shift vertically by an amount that is approximately independent of the atomic number *Z*. For the DR process, however, there are some differences, that is, if one did not consider the *E*1-*M*2 interference effects, the polarization of the *E*1 component would equal a constant 0.6, and the *M*2 component would equal a constant −1 (not shown in the figure). As shown in figure 2(b), a strong variation in the linear polarization is found if the *E*1-*M*2 interference effects are taken into account. The *E*1-*M*2 interference effects make linear polarization decrease rapidly, features that become more evident as the atomic number increases.

In order to illustrate the *E*1-*M*2 interference on the polarization properties more clearly, in figure 3 we show the dependence of the polarization degree of the $1s_{1/2}\ 2s_{1/2}\ 2p_{3/2}$ $(J = 3/2) \rightarrow\ 1s^2 2s_{1/2}(J = 1/2)$ transition line of Li-like $U^{89+}$ ions at 1.2 times the threshold energy formed by EIE and DR processes on the angle $\theta$ between the observation direction and the electron beam, respectively. It is found that the maximum polarization occurs at $\theta = 90°$ in all cases and the differences between the polarization of the *E*1 component and the *M*2 component become increasingly pronounced as $\theta$ tends to 90°. It is also found that the linear polarization of the *E*1 component is smaller than the absolute value of the *M*2 component over a wide range of angles, especially for the DR process. The *E*1-*M*2 interference effects can reduce the angular distribution of the linear polarization of the *E*1 component for Li-like $U^{89+}$ ions by about 15% and 21.7% for EIE and DR processes, respectively.

To examine the *E*1-*M*2 interference effects on the angular distribution of subsequent x-ray photoemission, in figure 4 we show the $W(\theta)/\langle W\rangle$ ratios of the $1s_{1/2}2s_{1/2}2p_{3/2}$ $(J = 3/2) \rightarrow 1s^2 2s_{1/2}(J = 1/2)$ line at 1.2 times the threshold energy formed by EIE and DR processes versus angle $\theta$, respectively. A comparison of the *E*1-*M*2 results and the *E*1 results in both figures 4(a) and 4(b) shows clearly that inclusion of the *E*1-*M*2 interference in calculations leads to a reduction in the anisotropy of the intensity angular distribution, which is contrary to the polarization. This reduction is more significant for the DR process than the EIE process. The contributions of *E*1-*M*2 interference effects on the polarization of the *E*1 component for Li-like $U^{89+}$ ions are about 3% and 8% for EIE and DR processes, respectively. Moreover, the interference causes a change in the angular distribution of photoemission in the $W(\theta)/\langle W\rangle$ ratio for the *M*2 result. That is to say, the *M*2 result leads to a dominant photon emission along the electron beam at small angle $\theta$, while including the *E*1-*M*2 interference clearly favors an emission perpendicular to the electron beam.

### *3.3. The contributions of the magnetic quadrupole to He-like $U^{90+}$ ions*

In the above sections, we have discussed the effects of *E*1-*M*2 interference on the polarization properties and angular

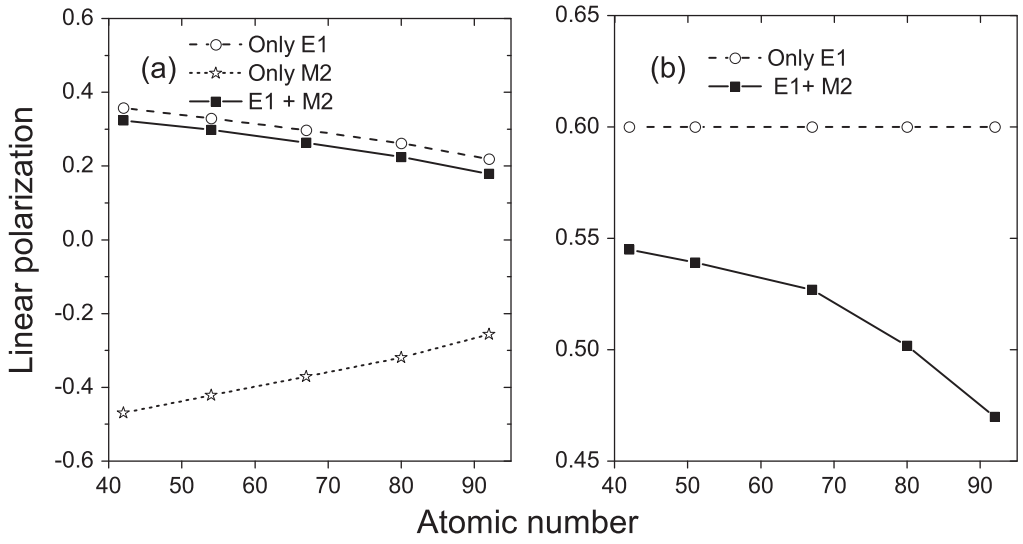


**Figure 2.** The linear polarization at the observation angle of 90° for the transition line $1s_{1/2}2s_{1/2}2p_{3/2}\,(J = 3/2) \rightarrow 1s^2 2s_{1/2}(J = 1/2)$ of Li-like ions following EIE (left) at 1.2 times the threshold energy and DR (right) processes as functions of the atomic number. E1 represents inclusion of only the electric-dipole approximation, M2 represents inclusion of only the magnetic-quadrupole approximation, and E1+M2 represents values with inclusion of *E1-M2* interference.

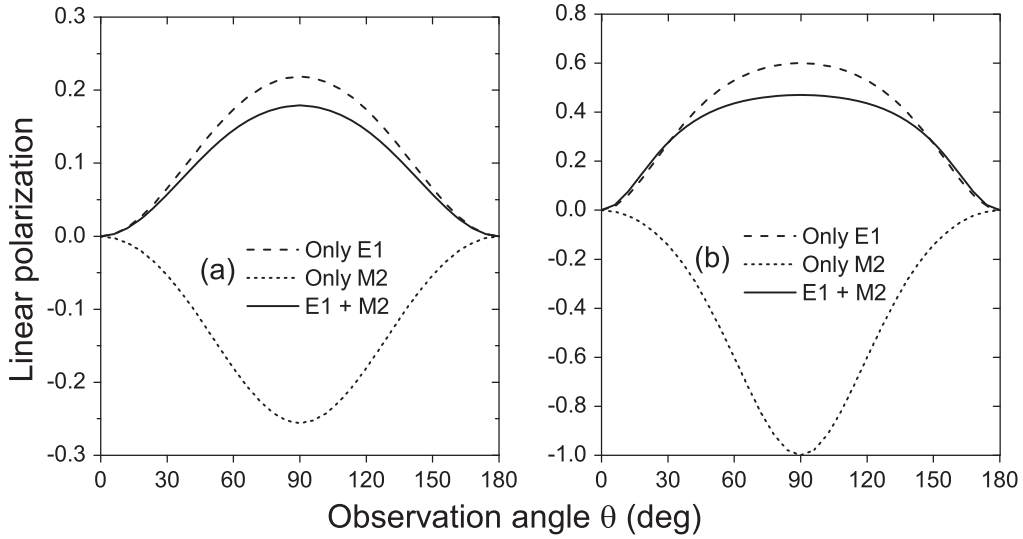


**Figure 3.** The degree of linear polarization of the transition line $1s_{1/2}\ 2s_{1/2}\ 2p_{3/2}(J=3/2) \rightarrow 1s^2 2s_{1/2}(J=1/2)$ for Li-like $U^{89+}$ ions following EIE (left) and DR (right) processes as a function of the observation angle $\theta$ relative to the electron beam. E1 represents inclusion of only the electric-dipole approximation, M2 represents inclusion of only the magnetic-quadrupole approximation, and E1+M2 represents values with inclusion of *E*1-*M*2 interference.

distribution of Li-like $U^{89+}$ ions for the decay from individual magnetic sublevels to the ground state $1s^2 2s_{1/2}(J = 1/2)$. In further studies we will pay attention to the decay from individual magnetic sublevels to the metastable state $1s_{1/2}2s_{1/2}(J = 1)$. In figure 5, we show the influence of the *E*1-*M*2 interference on the degree of linear polarization as functions of incident electron energy for the $2s_{1/2}3p_{3/2}\,(J = 1) \rightarrow 1s_{1/2}2s_{1/2}(J = 1)$ transition line of He-like $U^{90+}$ ions following the EIE process. It is found that the polarization of the *E*1 radiation component is equal to that of the *M*2 one. Therefore, without allowance for the *E*1-*M*2 interference effects, there is no partial cancellation between the *E*1 and *M*2 contributions in both polarization properties and angular distribution [41]. It is also found that the *E*1-*M*2 interference effects cause the linear polarization to decrease at an energy range below 1.3 times the threshold energy before starting to increase at higher energies. Polarizations with and without interference effects cross each other at 1.31 times the threshold energy. The *E*1-*M*2 interference effects can increase the linear polarization of the *E*1 component for He-like $U^{90+}$ ions by about 43% at three times the threshold energy.

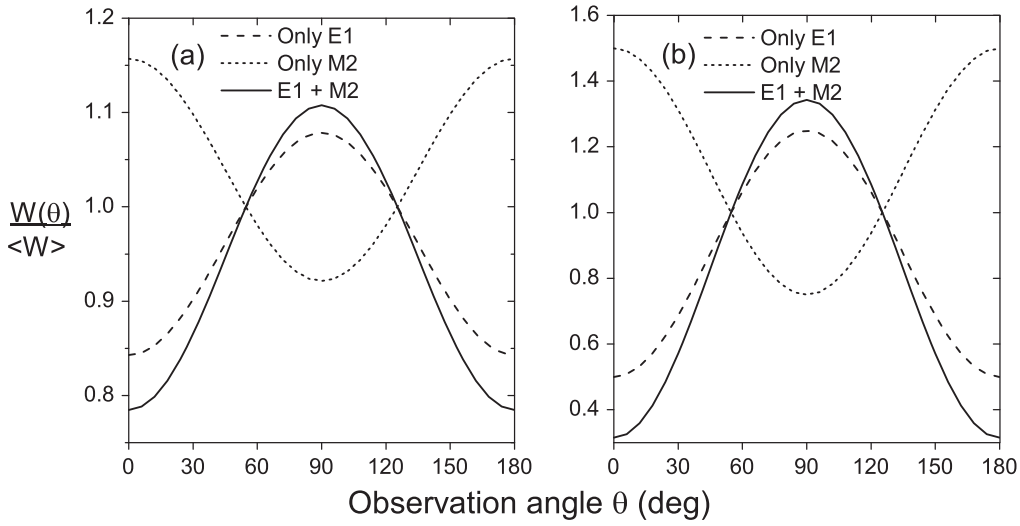


**Figure 4.** W($\theta$)/⟨ W ⟩ ratio for the transition line $1s_{1/2}\ 2s_{1/2}\ 2p_{3/2}(J=3/2) \rightarrow 1s^2 2s_{1/2}(J=1/2)$ for Li-like $U^{89+}$ ions following EIE (left) and DR (right) processes as a function of the observation angle $\theta$ relative to the electron beam. E1 represents inclusion of only the electric-dipole approximation, M2 represents inclusion of only the magnetic-quadrupole approximation, and E1+M2 represents values with inclusion of $E1$-$M2$ interference.

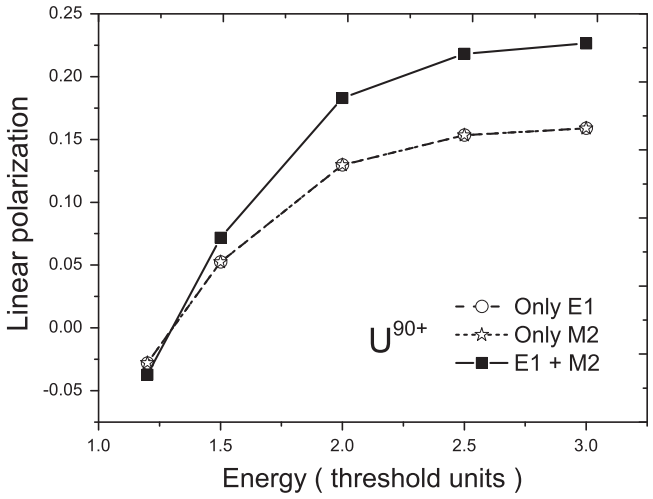


**Figure 5.** The linear polarization at the observation angle of 90° for the transition line $2s_{1/2}\ 3p_{3/2}(J=1) \rightarrow 1s_{1/2}\ 2s_{1/2}(J=1)$ of He-like $U^{90+}$ ions following the EIE process as functions of the incident electron energy in threshold units. E1 represents inclusion of only the electric-dipole approximation, M2 represents inclusion of only the magnetic-quadrupole approximation, and E1+M2 represents values with inclusion of $E1$-$M2$ interference.

In figure 6, we show the polarizations for the $2s_{1/2}3p_{3/2}\,(J=1) \rightarrow 1s_{1/2}2s_{1/2}\,(J=1)$ transition line of He-like ions at three times the threshold energy formed by EIE and DR processes versus the atomic number, respectively. In the figure, we can clearly find that the $E1$-$M2$ interference effects increase the degree of linear polarization for the EIE process, while decreasing it for the DR process. We can also find that the differences between the linear polarization with and without $E1$-$M2$ interference effects at the given energies become more evident as the atomic number increases. Figure 7 shows the dependence of the linear polarization degree of the $2s_{1/2}3p_{3/2}(J=1) \rightarrow 1s_{1/2}\ 2s_{1/2}(J=1)$ transition line of He-like $U^{90+}$ ions at three times the threshold energy formed by EIE and DR processes on the angle $\theta$, respectively. It is found that the angular distribution of linear polarization has the opposite sign for EIE and DR processes. The contributions of $E1$-$M2$ interference effects to the linear polarization of the $E1$ component for the He-like $U^{90+}$ ions are about 38% and 20% for EIE and DR processes, respectively.

Finally, in figure 8, we show the W($\theta$)/⟨ W ⟩ ratios of the $2s_{1/2}3p_{3/2}\,(J=1) \rightarrow 1s_{1/2}2s_{1/2}(J=1)$ line of He-like $U^{90+}$ ions formed by the EIE process versus angle $\theta$ at three times the threshold energy. As shown in figure 8, $E1$-$M2$ interference effects lead to a reduction in the anisotropy of the angular distribution of radiation. And the dominant photon emission perpendicular to the electron beam, the inclusion of $E1$-$M2$ interference, clearly favors a collinear emission along the electron beam [41], contrary to Li-like $U^{89+}$ ions. These characteristics are very similar to the conclusions for the linear polarization of the other radiative radiations formed by the DR process [32].

Until now we have investigated the cross section and linear polarization following direct EIE. Admittedly, the resonance EIE may affect the linear polarizations in some cases [20]. However, according to our estimates, the resonance mainly comes from relatively high levels in the present energy region. So the contributions of the resonance effects to excitation cross sections and the linear polarizations should be small. Moreover, for the DR process, other contributions such as radiative recombination (RR) may be important in the cross sections. Because DR is the dominant mechanism for populating the upper magnetic sublevel and the background corresponding to the RR contribution can be removed from the investigative polarization properties of x-ray emission following

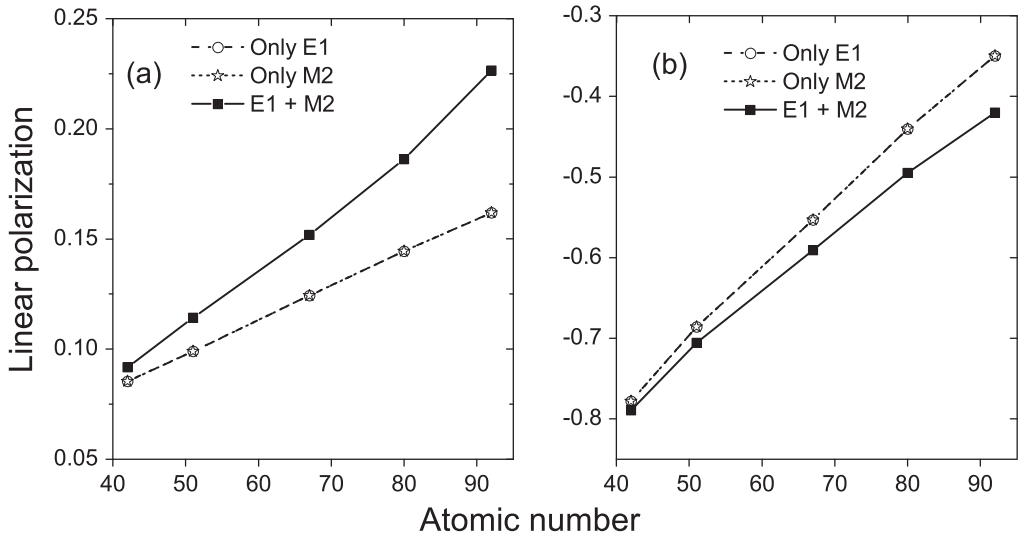


**Figure 6.** The linear polarization at the observation angle of 90° for the transition line $2s_{1/2}\ 3p_{3/2}(J=1) \rightarrow\ 1s_{1/2}\ 2s_{1/2}(J=1)$ of He-like ions following EIE (left) at three times the threshold energy and DR (right) processes as functions of the atomic number. E1 represents inclusion of only the electric-dipole approximation, M2 represents inclusion of only the magnetic-quadrupole approximation, and E1+M2 represents values with inclusion of *E*1-*M*2 interference.

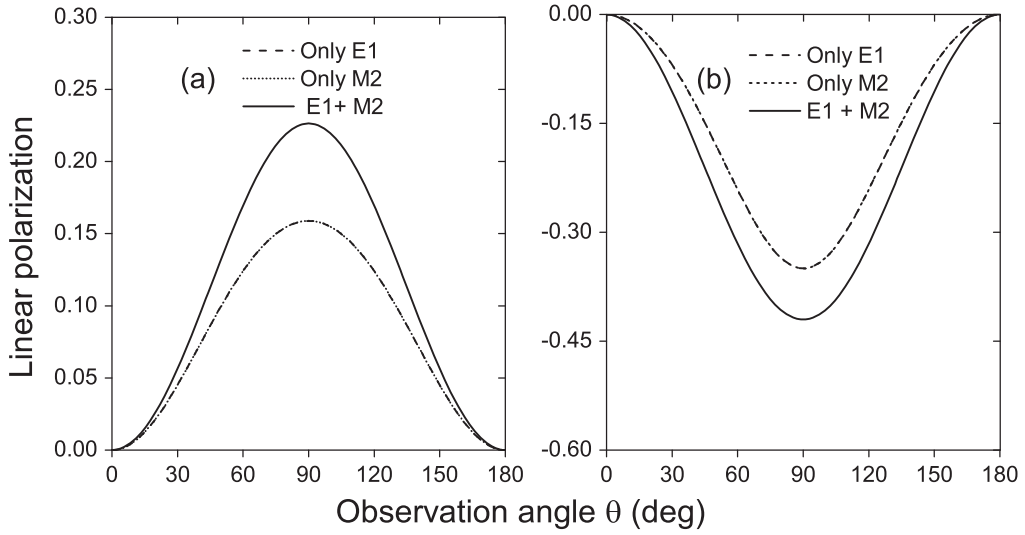


**Figure 7.** The degree of linear polarization of the transition line $2s_{1/2}\ 3p_{3/2}(J=1) \rightarrow\ 1s_{1/2}\ 2s_{1/2}(J=1)$ for He-like $U^{90+}$ ions following EIE (left) and DR (right) processes as a function of the observation angle $\theta$ relative to the electron beam. E1 represents inclusion of only the electric-dipole approximation, M2 represents inclusion of only the magnetic-quadrupole approximation, and E1+M2 represents values with inclusion of *E*1-*M*2 interference.

DR [14]. These effects are neglected in the present calculations.

## 4. Conclusions

Detailed calculations using a fully RDW method have been carried out for the linear polarization and angular distribution of x-ray radiation for the $2s_{1/2}\ 3p_{3/2}(J = 1) \rightarrow 1s_{1/2}\ 2s_{1/2}(J = 1)$ transition line of He-like $U^{90+}$ ions and the $1s_{1/2}\ 2s_{1/2}\ 2p_{3/2}\ (J = 3/2) \rightarrow 1s^2 2s_{1/2}(J = 1/2)$ transition line of Li-like $U^{89+}$ ions formed by EIE and DR processes, respectively. Special attention has been paid to the comparisons of the contributions of *M*2 decay to the polarization properties and angular distribution of radiation for subsequent x-ray emission from the above two different processes. Our results show that quantum interference effects between the *E*1 and *M*2 decay channels may significantly enhance the linear polarization of the $2s_{1/2}\ 3p_{3/2}(J = 1) \rightarrow 1s_{1/2}\ 2s_{1/2}(J = 1)$ transition line and decrease the linear polarization of the $1s_{1/2}\ 2s_{1/2}\ 2p_{3/2}(J = 3/2) \rightarrow 1s^2 2s_{1/2}(J = 1/2)$ transition line. Such dramatic influence also leads to a remarkable variation in the subsequent angular emission pattern. All these effects are slight for EIE but substantial for the DR process. We hope the present

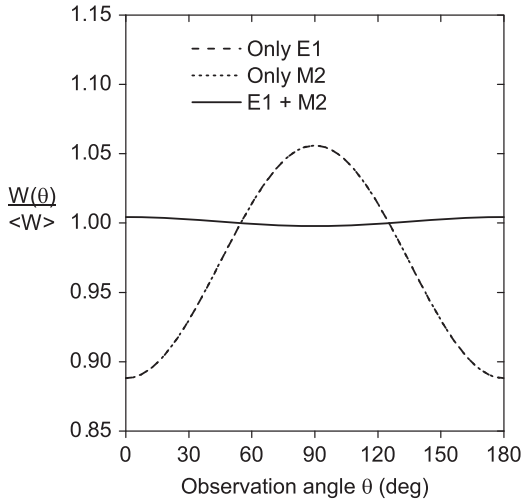


**Figure 8.** $W(\theta)/\langle W \rangle$ ratio for the transition line $2s_{1/2}\ 3p_{3/2}(J=1) \rightarrow 1s_{1/2}\ 2s_{1/2}(J=1)$ for He-like $U^{90+}$ ions following the EIE process as a function of the observation angle $\theta$ relative to the electron beam. E1 represents inclusion of only the electric-dipole approximation, M2 represents inclusion of only the magnetic-quadrupole approximation, and E1+M2 represents values with inclusion of *E*1-*M*2 interference.

results will stimulate interest in performing such interference experiments. These would open new possibilities of probing in a sensitive way the electron-photon interaction in highly charged ions.

## Acknowledgments

This work was supported by the National Natural Science Foundation of China (grant no. 11274382, no.11274254, and no. U1332206).

## References

[1] Dubau J, Inal M K and Urnov A M 1996 *Phys. Scr.* **T65** 179
[2] Haug E 1979 *Sol. Phys.* **61** 129
[3] Shlyaptseva A S, Hansen S B, Kantsyrev V L, Bauer B S, Fedin D A, Ouart N, Kazantsev S A, Petrashen A G and Safronova U I 2001 *Rev. Sci. Instrum.* **72** 1241
[4] Kieffer J C, Matte J P, Pépin H, Chaker M, Beaudoin Y, Johnston T W, Chien C Y, Coe S, Mourou G and Dubau J 1992 *Phys. Rev. Lett.* **68** 480
[5] Kieffer J C, Matte J P, Chaker M, Beaudoin Y, Chien C Y, Coe S, Mourou G, Dubau J and Inal M K 1993 *Phys. Rev.* E **48** 4648
[6] Hakel P, Mancini R C, Gauthier J-C, Mínguez E, Dubau J and Cornille M 2004 *Phys. Rev.* E **69** 056405
[7] Chen Z B, Dong C Z, Xie L Y and Jiang J 2014 *Phys. Rev.* A **90** 012703
[8] Shi Y L, Dong C Z, Ma X Y, Wu Z W, Xie L Y and Fritzsche S 2013 *Chin. Phys. Lett.* **30** 063401
[9] Reed K J and Chen M H 1993 *Phys. Rev.* A **48** 3644
[10] Hakel P, Mancini R C, Harris C, Neill P, Beiersdorfer P, Csanak G and Zhang H L 2007 *Phys. Rev.* A **76** 012716
[11] Sharma L, Surzhykov A, Srivastava R and Fritzsche S 2011 *Phys. Rev.* A **83** 062701
[12] Inal M K, Sampson D H, Zhang H L and Dubau J 1997 *Phys. Scr.* **55** 170
[13] Fritzsche S, Surzhykov A and Stöhlker T 2009 *Phys. Rev. Lett.* **103** 113001
[14] Hu Z, Han X, Li Y, Kato D, Tong X and Nakamura N 2012 *Phys. Rev. Lett.* **108** 073002
[15] Matula O, Fritzsche S, Currell F J and Surzhykov A 2011 *Phys. Rev.* A **84** 052723
[16] Wu Z W, Dong C Z and Jiang J 2012 *Phys. Rev.* A **86** 022712
[17] Amaro P, Fratini F, Fritzsche S, Indelicato P, Santos J P and Surzhykov A 2012 *Phys. Rev.* A **86** 042509
[18] Inal M K, Surzhykov A and Fritzsche S 2005 *Phys. Rev.* A **72** 042720
[19] Kai T, Nakazaki S, Kawamura T, Nishimura H and Mima K 2007 *Phys. Rev.* A **75** 012703
[20] Jiang J, Dong C Z, Xie L Y and Wang J G 2008 *Phys. Rev.* A **78** 022709
[21] Beiersdorfer P *et al* 1996 *Phys. Rev.* A **53** 3974
[22] Takács E *et al* 1996 *Phys. Rev.* A **54** 1342
[23] Nakamura N, Kato D, Miura N, Nakahara T and Ohtani S 2001 *Phys. Rev.* A **63** 024501
[24] Robbins D L *et al* 2006 *Phys. Rev.* A **74** 022713
[25] Itikawa Y, Srivastava R and Sakimoto K 1991 *Phys. Rev.* A **44** 7195
[26] Inal M K and Dubau J 1987 *J. Phys. B: At. Mol. Phys.* **20** 4221
[27] Surzhykov A, Litvinov Y, Stöhlker T and Fritzsche S 2013 *Phys. Rev.* A **87** 052507
[28] Safari L, Amaro P, Fritzsche S, Santos J P, Tashenov S and Fratini F 2012 *Phys. Rev.* A **86** 043405
[29] Safari L, Amaro P, Fritzsche S, Santos J P and Fratini F 2012 *Phys. Rev.* A **85** 043406
[30] Safari L, Amaro P, Santos J P and Fratini F 2014 *Phys. Rev.* A **90** 014502
[31] Surzhykov A, Fritzsche S, Gumberidze A and Stöhlker T 2002 *Phys. Rev. Lett.* **88** 153001
[32] Fritzsche S, Kabachnik N M and Surzhykov A 2008 *Phys. Rev.* A **78** 032703
[33] Fritzsche S, Surzhykov A and Stöhlker T 2011 *Phys. Scr.* **T144** 014002
[34] Surzhykov A, Sharma L, Stöhlker T and Fritzsche S 2010 *Journal of Physics: Conference Series* **212** 012032
[35] Weber G *et al* 2010 *Phys. Rev. Lett.* **105** 243002
[36] Parpia F A, Fischer C F and Grant I P 1996 *Comput. Phys. Commun.* **94** 249
[37] Fritzsche S, Aksela H, Dong C Z, Heinäsmäki S and Sienkiewicz J E 2003 *Nucl. Instrum. Methods Phys. Res.* B **205** 93
[38] Chen Z B, Zeng J L and Dong C Z 2015 *J. Phys. B: At. Mol. Opt. Phys.* **48** 045202
[39] Wu Z W, Dong C Z and Jiang J 2011 *Phys. Rev.* A **84** 032713
[40] Zhang H L, Sampson D H and Clark R E H 1990 *Phys. Rev.* A **41** 198
[41] Bensaid R, Inal M K and Dubau J 2006 *J. Phys. B: At. Mol. Phys.* **39** 4131
[42] http://astronomy.ohio-state.edu/~nahar/nahar_radiativeatomicdata/index.html
[43] Nahar S N, Pradhan A K and Lim S 2011 *Can. J. Phys.* **89** 483
[44] http://nist.gov/pml/data/asd.cfm
[45] Hata J and Grant I P 1984 *Mon. Not. R. Astr. Soc.* **211** 549